

Marquette University

e-Publications@Marquette

Civil and Environmental Engineering Faculty
Research and Publications

Civil, Construction, and Environmental
Engineering, Department of

12-2018

Development of Domain Analysis to Predict Multi-Axial Flexible Airfield Pavement Responses Due to Gear and Environmental Loadings

Angeli Gamez

University of Illinois at Urbana-Champaign

Jaime Hernandez

Marquette University, jaime.hernandez@marquette.edu

Imad L. Al-Qadi

University of Illinois - Urbana-Champaign

Follow this and additional works at: https://epublications.marquette.edu/civengin_fac



Part of the [Civil Engineering Commons](#)

Recommended Citation

Gamez, Angeli; Hernandez, Jaime; and Al-Qadi, Imad L., "Development of Domain Analysis to Predict Multi-Axial Flexible Airfield Pavement Responses Due to Gear and Environmental Loadings" (2018). *Civil and Environmental Engineering Faculty Research and Publications*. 300.

https://epublications.marquette.edu/civengin_fac/300

Marquette University

e-Publications@Marquette

Civil and Environmental Engineering Faculty Research and Publications/College of Engineering

This paper is NOT THE PUBLISHED VERSION.

Access the published version via the link in the citation below.

Transportation Research Record : Journal of the Transportation Research Board, Vol. 2672, No. 40 (December 2018): 236-335. [DOI](#). This article is © National Academy of Sciences and permission has been granted for this version to appear in [e-Publications@Marquette](#). National Academy of Sciences does not grant permission for this article to be further copied/distributed or hosted elsewhere without express permission from National Academy of Sciences.

Development of Domain Analysis to Predict Multi-Axial Flexible Airfield Pavement Responses Due to Gear and Environmental Loadings

Angeli Gamez

University of Illinois at Urbana-Champaign, Illinois Center for Transportation, Rantoul, IL

Jaime A. Hernandez

University of Illinois at Urbana-Champaign, Illinois Center for Transportation, Rantoul, IL

Imad L. Al-Qadi

University of Illinois at Urbana-Champaign, Illinois Center for Transportation, Rantoul, IL

Abstract

Flexible pavement design procedures use maximum mechanistic strains to predict service life via empirical transfer functions. The conventional method of using predefined point locations for potential damage may not accurately represent realistic pavement scenarios. For instance, flexible airfield pavement analysis mainly considers the critical strain at the bottom of the asphalt concrete (AC), which may not characterize near-surface cracking potential. In lieu of point strains, domain analysis, a new method, accounts for the multi-axial behavior of pavements, as inherently excited by three-dimensional (3-D) and nonuniform aircraft tire–pavement contact stresses. Initially applied on highway pavements considering truck tire loading, this approach is an initial breakthrough for implementing domain analysis on flexible airfield pavements; in this study, A-380 and F-16 landing gear tire loads were considered. As anticipated, speed and temperature had significant influence on cumulative domain stress and strain ratios. The decrease in speed and increase in temperature not only increased the cumulative ratios up to 1.81, but nonlinearity of the problem became more prevalent at worst loading conditions (8 kph and 45°C). Minimal difference in ratios for F-16 cases suggests that the National Airport Pavement Test Facility pavement structure became less sensitive to conditions under low loads. Point response analysis revealed that critical strains were not significantly influenced by the tire-inflation pressure, for example, tensile strain at the bottom of the AC only increased up to 13.6% (considering 8 kph speed), whereas domain analysis quantified the increase with respect to 3-D stress or strain states.

Conventional flexible airfield pavement design procedure utilizes the maximum vertical strain at the top of the subgrade and maximum horizontal strain at the bottom of asphalt concrete (AC) layers to predict pavement structural life. Similar to highway pavement design, transfer functions relate mechanistic strains to empirical equations to determine the total number of load cycles that a pavement structure can withstand prior to failure (1). The Federal Aviation Administration (FAA) has developed the publicly available software FAARFIELD to design pavements considering airplane characteristics, including loading gear type and geometry, tire-inflation pressure, and traffic volume. Although FAARFIELD implements a multilayered elastic and three-dimensional (3-D) finite element (FE)-based design procedure, several inputs are simplified. For instance, AC is characterized as an elastic layer and for the aircraft tire loading, the contact pressure is assumed equivalent to the tire-inflation pressure (uniformly distributed over a circular or rectangular contact area).

FE modeling is a robust tool used by the scientific community to simulate complex problems (e.g., airfield pavement analysis). In contrast to analytical models, 3-D FE pavement modeling capabilities include multi-axial tire–pavement contact stresses, viscoelastic and nonlinear material characterization, material damping, layer interface properties, dynamic analysis, infinite boundary, and continuously moving load (2–5). All the aforementioned considerations provide a step forward in simulating a realistic loaded pavement scenario.

Furthermore, flexible pavement test sections have been studied to determine the effect of numerous variables on pavement behavior, including aircraft tire load, temperature, traveling speed, and tire-inflation pressure. Garg and Hayhoe reported their findings from the National Airport Pavement Test Facility (NAPTF), that the increase in temperature and decrease in speed excite the viscous deformation more significantly than elastic deformation (6). The increase in the temperature from

11.1°C to 22.2°C resulted in an increase in strains ranging from 100% to 120%. In addition, Al-Qadi and co-authors measured in-situ responses of an airport runway with actual airplane traffic (7), wherein the data were later used to validate a 3-D FE airfield pavement model (4). The magnitude of actual aircraft loads was a clear governing factor to trigger high levels of measured stresses and strains. Roginski indicated that high tire pressure had minimal adverse effect on pavement responses within the upper layer (8). A later study by Wang and co-authors determined that for an A-380 tire, an increase in tire-inflation pressure from 1.45 to 1.69 MPa caused 9% to 11% increase in maximum shear and compressive strains within the AC layer (9); however, these responses are not considered within the conventional design method.

A recent study dealing with truck tires revealed that point strains cannot adequately represent the multidimensional state of stresses and strains within a loaded pavement structure (10). Although an increase in tire-inflation pressure is expected to directly influence pavement behavior as the tire–pavement contact stress distribution is altered, the maximum strains did not change significantly. To address this issue, a new method, domain analysis, was developed to account for 3-D and nonuniform pavement responses that directly manifest from applied tire–pavement contact stresses (5,11–17). This paper aims to implement the domain analysis on an FE airfield pavement model considering the influence of varying AC surface temperatures, traveling speeds, and tire-inflation pressures for A-380 and F-16 tire loads. Utilizing the same FE airfield pavement output database, critical strain responses at point locations were extracted and compared with the 3-D cumulative stress and strain ratios. Details of the FE model and the domain analysis procedure are described in later sections. The paper concludes by highlighting the advantages of the domain analysis outputs over point responses.

FE Model

A NAPTF flexible airfield pavement structure was simulated using Abaqus. Previously constructed in the High Tire Pressure test area at NAPTF (18), the pavement structure consists of 125 mm of AC (P401), 200 mm of crushed stone base (P209), 150 mm of Econcrete (P306), and 810 mm of uncrushed stone (P154) (19). These material notations are used in later sections. Regarding material properties, AC was assumed as linear viscoelastic, while the supporting layers below the crushed stone base were characterized as linear elastic. On the other hand, a nonlinear, isotropic, and stress-dependent model was implemented for the crushed stone base layer due to high stress levels excited by aircraft tire loads.

In addition, a mesh sensitivity analysis was completed to determine optimum discretization of the selected pavement structure with the criteria of balancing an acceptable level of accuracy with feasible computational effort. The FE pavement model considered AC temperature profiles, layer interface properties, infinite boundary elements for far-field region behavior (20), continuously moving load (2), and nonuniform contact stresses. Details of the FE model, including material properties and mesh sensitivity analysis, are discussed elsewhere (21).

Analysis Matrix

Three-dimensional and nonuniform contact stresses from a single landing gear of the A-380 and F-16 aircrafts were considered in this study. The tire loads for A-380 and F-16 were assumed constant at 262 and 72 kN, respectively. The numerical matrix included three traveling speeds (8, 140, and 270 kph)

and three AC surface temperatures (−12, 21, and 45°C). Tire-inflation pressures also varied; however, appropriate values were assumed for each aircraft tire. The A-380 landing gear tire-inflation pressures were assumed to be 1.45 and 1.69 MPa; for the F-16 landing gear, tire-inflation pressures were assumed to be 2.14 and 2.41 MPa. A total of 36 numerical simulations were conducted using computing resources from the Extreme Science and Engineering Discovery Environment (22). It is important to recall that the analysis is constrained to consider the AC layer as a viscoelastic material, although under the worst loading conditions (slow speed, high tire-inflation pressure, and high load) AC materials tend to exhibit more viscoplastic behavior. Given that the FE model considers a 3-D moving load, stress-dependency of the base material, and dynamic analysis, incorporating viscoplasticity as a part of the structural analysis would be computationally infeasible at the current time.

Tire–Pavement Contact

Representing the tire–pavement contact stresses for the A-380 and F-16 as 3-D and nonuniform, the distribution of vertical contact stresses along each rib σ_z was calculated using (23–25):

$$\sigma_z(x) = \frac{\alpha L}{lb} \left(1 + \frac{1}{2n}\right) \left[1 - \left(2\frac{x}{l} - 1\right)^{2n}\right]$$

where L is the applied load; l is the contact length; b is the rib width; x is the distance along contact length; α is the percentage of L carried by a rib; and n is the shape parameter of $\sigma_z(x)$. The maximum vertical contact stresses were assumed to occur at the center of the contact length (this might be slightly inaccurate for high speed) by assigning the shape parameter as follows:

$$n = \frac{1}{2 \left(\frac{lb\sigma_{z,max}}{\alpha L} - 1 \right)}$$

where $\sigma_{z,max}$ is the maximum vertical contact stress along the corresponding rib.

Results reported within the literature defined the contact area details. The contact patch of the A-380 tire comprised five ribs, wherein the assumed width of the exterior and middle ribs were 90 and 70 mm, respectively, and the width of the other ribs was 45 mm. A contact length of 560 mm was implemented for all ribs (26). Contact area details for the F-16 were based on results reported by Lindsley and co-authors (27). Five 240 mm long ribs composed the contact patch; the widths for the exterior and middle ribs were 30 mm and for the other ribs were 20 mm. To determine the distribution of σ_z along the contact length, the ratio between the maximum σ_z and tire-inflation pressure was assumed. The ratios for A-380 cases were 1.8 for the two exterior ribs, and 1.1 for the three interior ribs; the F-16 cases considered 1.7 and 1.3 for the exterior and interior ribs, respectively.

Variations of the longitudinal and transverse contact stresses were defined based on experimental measurements from truck tires (28). Transverse contact stresses σ_y had the same shape as σ_z ; however, the magnitude was assigned as $0.40\sigma_z$ and applied only at the rib edges. Longitudinal contact stresses consisted of two skewed parabolas with a common point at $x = 0.85l$, and peak values of $\sigma_{x,max}=0.20 \sigma_{z,max}$ and $\sigma_{x,min}=-0.15 \sigma_{z,max}$ at $x = 0.20l$ and $x = 0.85l$, respectively (23). The

contact stresses along the vertical, longitudinal, and transverse directions for a representative rib of F-16 are presented in Figure 1. One could clearly observe the effect of tire-inflation pressure on the peak σ_z and shape of σ_z versus x curve wherein higher tire-inflation pressure resulted in larger and better-defined maximum vertical contact stresses. Details of the A-380 tire–pavement contact stresses are presented in a different publication (23). It is worth noting that the generated contact stress inputs reflect a free-rolling tire condition and are anticipated to change when other scenarios are considered. Special cases considering turning, braking, and accelerating conditions, which generate significantly different contact stresses mainly in the longitudinal direction (29), were not included as they are outside the scope of this study.

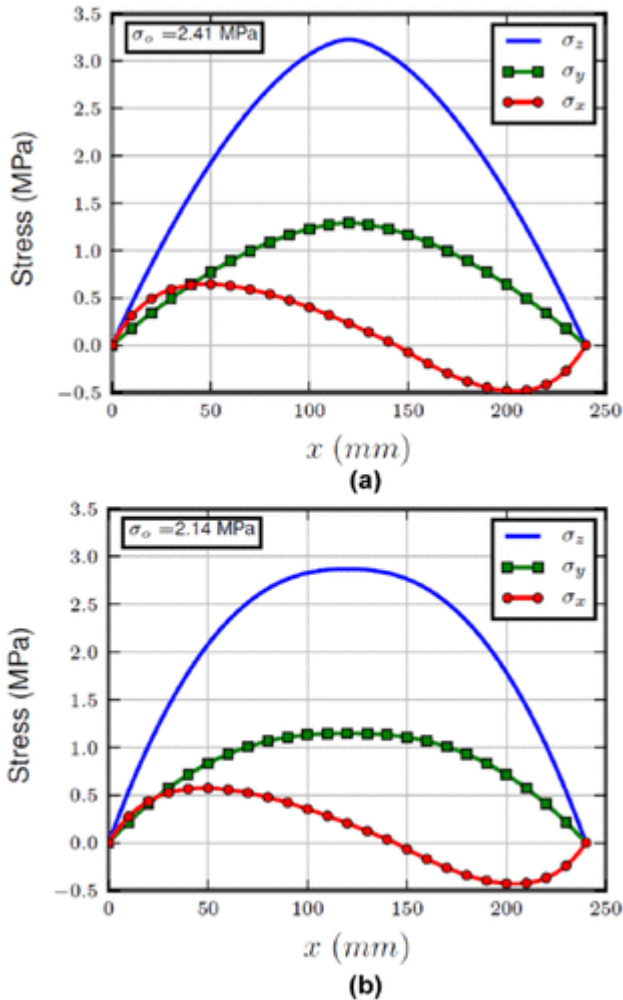


Figure 1. Three-dimensional contact stresses along the center rib of F-16 considering tire-inflation pressures of: (a) 2.14 MPa and; (b) 2.41 MPa.

FE Point Responses

FAA flexible pavement design relies upon two point responses: tensile strain at the bottom of the AC $\varepsilon_{11,ac}$ and vertical strain on top of the subgrade $\varepsilon_{22,sg}$ (1). The aforementioned strain responses relate to fatigue cracking within the AC and rutting within the subgrade, respectively; however, multiple critical pavement responses are associated with other pavement distresses. In particular, the transverse strain at the bottom of the AC $\varepsilon_{33,ac}$ influences bottom-up fatigue cracking; transverse

surface strain $\epsilon_{33,sf}$ affects near-surface cracking; and shear strain in each layer is related to rutting ($\epsilon_{23,ac}$, $\epsilon_{23,bs}$, $\epsilon_{23,P306}$, $\epsilon_{23,P154}$, and $\epsilon_{23,subg}$, subg for the vertical shear strain in the AC, base, P306, P154, and subgrade, respectively).

The aforementioned strain responses were extracted from airfield pavement simulations. Figure 2 presents the impact of tire-inflation pressure and speed on critical pavement responses, excited by F-16 tire loading (the same analysis scheme was applied for A-380 loading cases). The point responses along the horizontal axis are grouped and each bin consists of six bars; each bar represents a case considering a combination of speed and tire-inflation pressure. All the strain responses for each load case are normalized to a reference case, which considers the speed of 8 kph and tire-inflation pressure of 2.14 MPa (as indicated on the vertical axis description). For example, one could notice that the first bar, for each bin (left-most) within Figure 2, equates to unity as this is the reference case.

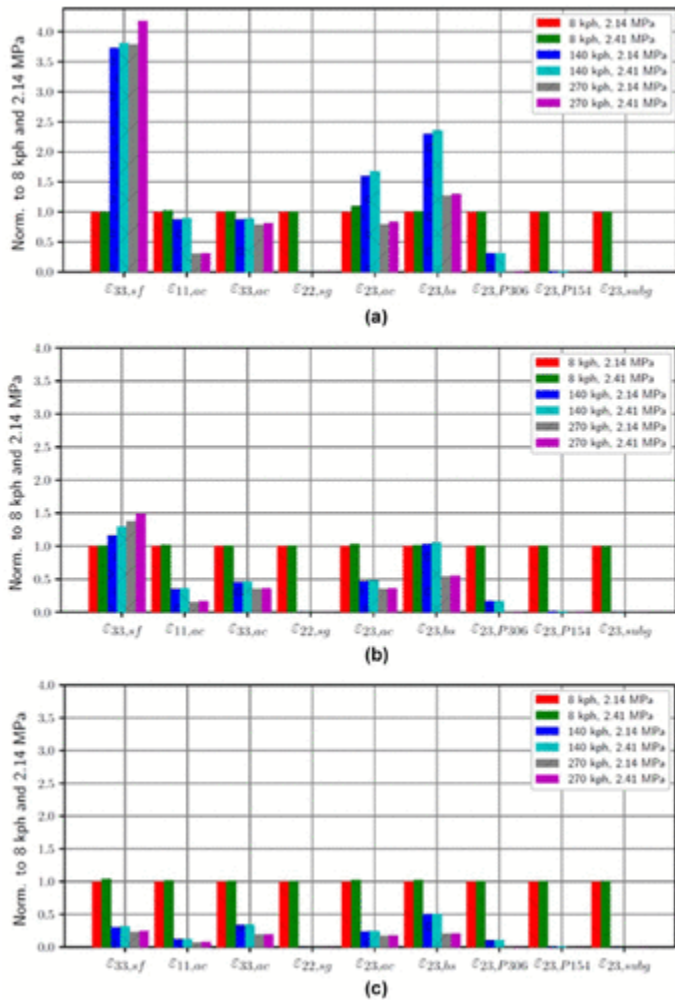


Figure 2. Critical pavement responses for F-16 considering AC surface temperatures of: (a) -12°C ; (b) 21°C and; (c) 45°C .

Expected trends, resulting from changes in temperature, speed, and tire-inflation pressure, were observed for both aircraft tire loads. First, as temperature increased from -12°C to 45°C , AC stiffness decreased, thus causing significantly higher strains. Second, in general, strains are reduced as speed increases because of the stiffening effect of speed on AC. And third, increasing tire-inflation pressure

resulted in higher pavement responses, although the difference between cases seemed irrelevant for multiple cases.

Specifically, changes in the tire-inflation pressure did not have significant influence on the tensile strain at the bottom of the AC, which is one of the two main design inputs considered by FAARFIELD. The increments in tire-inflation pressures were 13.4% and 12.6% for A-380 and F-16, respectively. At the lowest speed, $\varepsilon_{11,ac}$, for A-380 increased by 13.6% following the increase of tire-inflation pressure. The corresponding change for F-16 was much lower, wherein the greatest change was 3.1%. This smaller effect on F-16 is attributed to 27.5% lower tire loading than the A-380 cases on the same airfield pavement structure.

Strain responses are extracted from a single point location aligned with a specific direction. Furthermore, the traditional design procedure predetermines the location of potential damage initiation (only at two locations: bottom of AC and top of subgrade), which may not be true for all cases. Consequently, calculating damage using transfer functions unrealistically assumes negligible interaction between various damage mechanisms. These drawbacks, along with limited capability of point responses to capture the influence of tire-inflation pressures and near-surface responses, are addressed by the proposed method: domain analysis. Details of the new analysis scheme are presented in the following sections.

Domain Analysis Procedure

A new procedure, domain analysis, quantifies the multi-axial stress or strain states using a single scalar parameter. The proposed analysis scheme includes four main steps: (1) calculate multi-axial stress and strain states of a pavement structure; (2) discretize the pavement to identify critical zones; (3) compare stress and strain states with respect to the failure criteria; and (4) combine the failure potential of critical regions to obtain a scalar called cumulative ratio. A brief description of each step is presented; however, details of the domain analysis can be found elsewhere (10).

Multi-Axial Stress and Strain States

Stresses and strains are calculated using the simulated loaded airfield pavement structure. A subdomain is extracted from the FE pavement model to focus the analysis on critical regions, which envelops a volume with dimensions $1240 \times 962 \text{ mm}^2$ in the plan view and a depth of 2035 mm. Principal stresses and strains were utilized to compute the hydrostatic stress, p_σ , and shear stress indicator, q_σ , which can be calculated by

$$p_\sigma = \frac{1}{3}(\sigma_1 + \sigma_2 + \sigma_3)$$

$$q_\sigma = \sqrt{\frac{1}{2}[(\sigma_1 - \sigma_2)^2 + (\sigma_2 - \sigma_3)^2 + (\sigma_1 - \sigma_3)^2]}$$

where σ_1 , σ_2 , and σ_3 are the maximum, intermediate, and minimum principal stresses, respectively. In the following, the same form of equations can represent the hydrostatic strain, p_ε , and shear strain indicator, q_ε :

$$p_\varepsilon = \frac{1}{3}(\varepsilon_1 + \varepsilon_2 + \varepsilon_3)$$

$$q_\varepsilon = \sqrt{\frac{2}{9}[(\varepsilon_1 - \varepsilon_2)^2 + (\varepsilon_2 - \varepsilon_3)^2 + (\varepsilon_1 - \varepsilon_3)^2]}$$

where ε_1 , ε_2 , and ε_3 are the maximum, intermediate, and minimum principal strains, respectively. The hydrostatic and shear stress or strain indicator at each element centroid within the subdomain were plotted in a p - q diagram.

Domain Discretization

Relative to point strains, domain analysis aims to represent the spread of p - q coordinates within the 3-D subdomain. Another key part of the proposed method is to identify critical locations of potential pavement damage. Nine zones were identified, wherein the horizontal boundary is a function of the pavement layer thickness and the vertical boundary is defined by the tire width of a specific load case with an addition of 50 mm to both right and left sides to capture localization at tire edges. This addition corresponded to previous observations wherein high shear values localized near the tire edges (30, 31). Moreover, the horizontal boundary was confined within 100 mm from the surface, where near-surface cracking is generally observed (13). For simplicity, this horizontal boundary at the near-surface was mirrored to create zones at the bottom of the layer. Figure 3 presents the nine zones generated along the vertical cross-section.

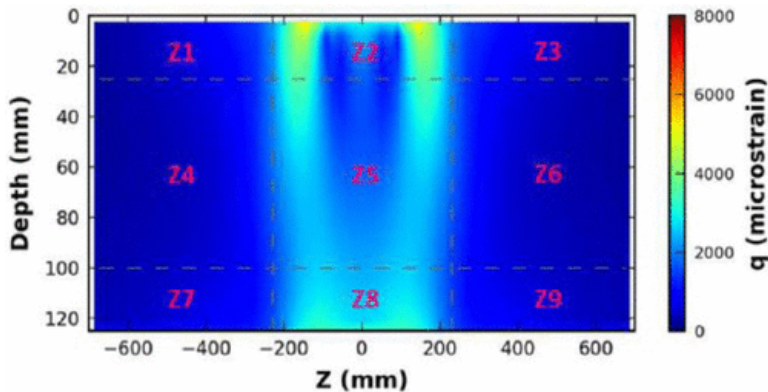


Figure 3. Zoning process.

In particular, six critical zones were considered to govern the analysis: (1) Z2 within the AC relating to near-surface cracking and rutting; (2) Z8 within the AC relating to bottom-up fatigue cracking; and (3) Z2 within the base, (4) Z2 within the Econcrete, (5) Z2 within the uncrushed stone base, and (6) Z2 within the subgrade related to rutting.

Inclusion of Failure Criteria

Using failure criteria, damage potential is quantified with respect to the current p - q state. The Modified Drucker–Prager Cap Model was selected as it accounts for tension cutoff, compression, and shear. It should be noted that any failure surface could be adapted within the domain analysis. Furthermore, the Cartesian coordinates of the p - q diagram were transformed into polar coordinates. The polar coordinate system was regionalized into 30 sectors, stemming from six radii and seven equally spaced angle boundaries. The rationale in the transformation is that polar sectors closest to the failure surface are penalized more than the ones farther away. The weights are defined by the stress or strain ratio (i.e., current stress or strain state of the sector midpoint divided by the allowable stress or strain state). A weight of 1.0 indicates that the midpoint sector coincides with the yield surface and failure is reached.

Cumulative Ratio

In the final step, a single scalar is calculated by considering geometry and adding all stress or strain states within the subdomain. A homogenizing factor was applied to account for the geometric difference between load cases along the vertical cross-sectional area. Using individual element area, a_{jl} , of element j within zone l and the total area, A_l , the homogenizing factor, a_{jl}/A_l is calculated.

Furthermore, another geometric difference could arise along the traveling direction. The element length, l_{elem} , is divided by the total length of the subdomain, L_{sub} , to obtain the volumetric factor, l_{elem}/L_{sub} . Using the vector magnitude of each p - q coordinate from the origin and weight factors, the p - q point cloud may be combined into a cumulative value, coined as the cumulative stress $C\sigma$ or cumulative strain $C\varepsilon$, which is calculated as follows:

$$C\sigma, \varepsilon_{case} = \frac{\sum_{l=1}^z \sum_{j=1}^e \sum_{i=1}^s |(pq)_{\sigma,\varepsilon}|_{jl} \times a_{jl} \times l_{elem} \times w_i}{A_l \times L_{sub}}$$

where $C\sigma, \varepsilon_{case}$ is the cumulative stress or strain of the specific load case; $|(pq)_{\sigma,\varepsilon}|_{jl}$ is the vector magnitude of the element j for a total of e elements within the zone l for a total of z zones; and w_i is the weight of the specific sector i for a total of s sectors.

The cumulative ratio is calculated as follows:

$$CRS = \frac{C\sigma_{case}}{C\sigma_{ref}}$$

$$CRE = \frac{C\varepsilon_{case}}{C\varepsilon_{ref}}$$

where CRS is the unitless cumulative ratio in the stress domain; CRE is the unitless cumulative ratio in the strain domain; $C\sigma_{ref}$ is the cumulative stress of the reference load case; and $C\varepsilon_{ref}$ is the cumulative strain of a reference load case. A sensitivity analysis of the zoning limits was completed to

evaluate their influence on the ratios. Although the cumulative stress or strain values were directly influenced, the cumulative ratios did not vary as significantly as the cumulative values. The trend of the ratios was also maintained despite the variation in zoning limits, which may be due to the fact that the two cases being compared (that form the ratio) utilize the exact same partitioning scheme. Future work may include determining a meaningful use of the cumulative values, along with the ratios.

Results and Discussion

Domain Analysis of A-380 Tire Load Cases

In contrast to point responses, the domain analysis accounts for the inherent 3-D response of a loaded pavement structure. For instance, Figure 4 illustrates the complex response of the stress-dependent base considering a single A-380 landing gear tire load and AC surface temperature of 45°C. Note that the p - q diagrams were extracted at a specific vertical cross-section along the subdomain contact length, where the maximum values were located. It is evident from the p - q cloud that an increase in the tire-inflation pressure by 17% led to significantly higher levels of compression and shear values.

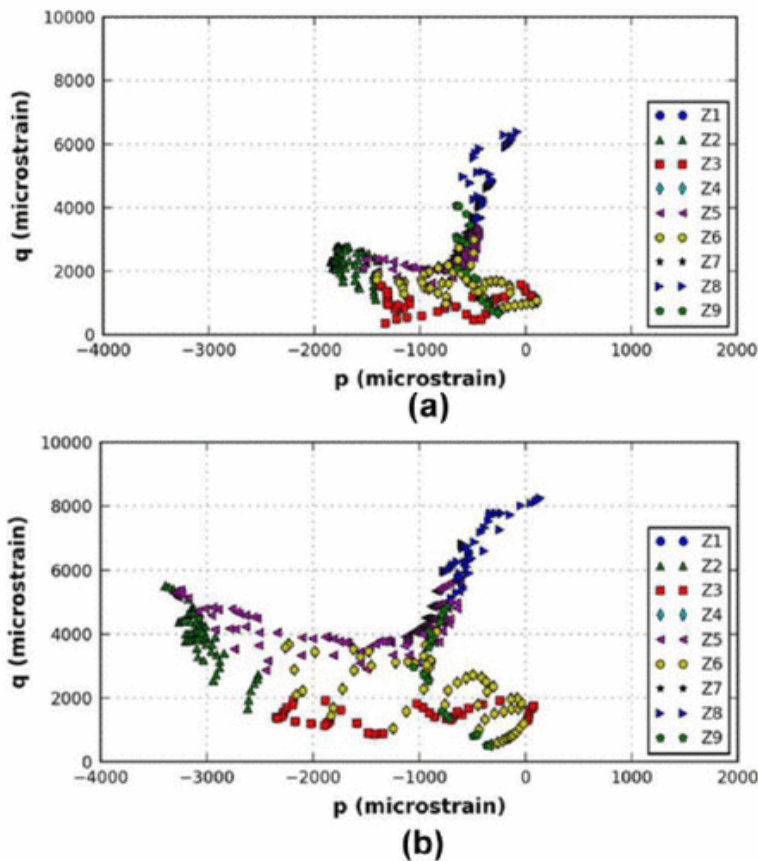


Figure 4. Case of A-380, p - q diagrams of loading cases with 8 kph, 45°C, and two tire-inflation pressure values: (a) 1.45 MPa and; (b) 1.69 MPa.

The outputs of the domain analysis include CRS and CRE values for each critical zone, and the weighted average of all the ratios from the selected six critical zones. The weighted average was calculated as a single metric to compare the numerical simulations. It is noteworthy that the loading cases were categorized with respect to the surface temperature and were normalized to the simulation

considering 8 kph speed and 1.45 MPa tire-inflation pressure. Hence, under the same AC temperature, *CRS* and *CRE* define the potential pavement damage relative to the normalizing load case.

A sample plot of the *CRS* and *CRE* values within the six critical zones is presented in Figure 5, considering an AC surface temperature of 21°C for varying tire speeds and inflation pressures. As the loading condition worsened, that is, decrease in speed and increase in tire-inflation pressure, the *CRS* at the near-surface and bottom zones of AC steadily increased from 0.20 to 1.36 (Figure 5a). Furthermore, the supporting layers below the granular base experienced significantly low stress or strain levels for cases considering tire speeds greater than 8 kph. Cumulative ratios within Z2 of P306, P154, and subgrade layers tended to zero, which indicates that the principal stresses and strains were also zero.

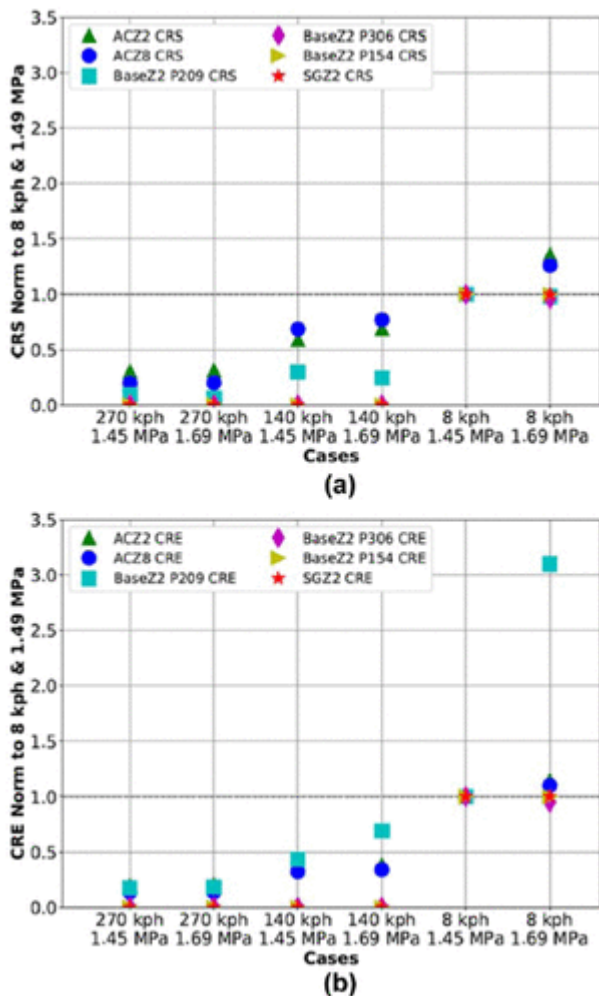


Figure 5. (a) *CRS* and (b) *CRE* within critical zones of A-380 cases considering 21°C AC surface temperature.

Most of the *CRE* values within the AC were significantly lower than those of the loading case under 8 kph and 1.45 MPa (Figure 5b). Under high speeds, AC layers tend to behave elastically. Conversely, as the loading speed reduced to 8 kph, the viscous components governed, leading to high strains. On the other hand, the base layer was relatively more sensitive to the changes in loading conditions as the *CRE* ranged from 0.17 to 3.1. Comparing the *CRE* trends with respect to AC surface temperatures,

the cases with -12°C revealed a steady increase, whereas the trend became highly nonlinear as the surface temperature further increased to 45°C .

An increase in the weighted average of the *CRS* was evident as the surface temperature increased from -12°C to 45°C , while the weighted average of the *CRE* decreased relative to the case under 8 kph and 1.45 MPa (Figure 6). This coincides with the rationale that at high temperatures, the stress state of the pavement structure becomes less sensitive to other parameters as temperature governs. The nonlinearity effect was also apparent as the disparity between *CRS* and *CRE* increased while the AC layer was subjected to higher temperatures. For instance, the *CRE* values for the cases considering 45°C varied between 0.05 and 1.7, wherein the considerable increase was observed under the speed of 8 kph. A clear change in the ratios as the tire-inflation pressure increased for each combination of speed and tire-inflation pressure is also presented in Figure 6. The importance of these findings supports the fact that the domain analysis appropriately captures the impact of the analysis variables on 3-D pavement responses.

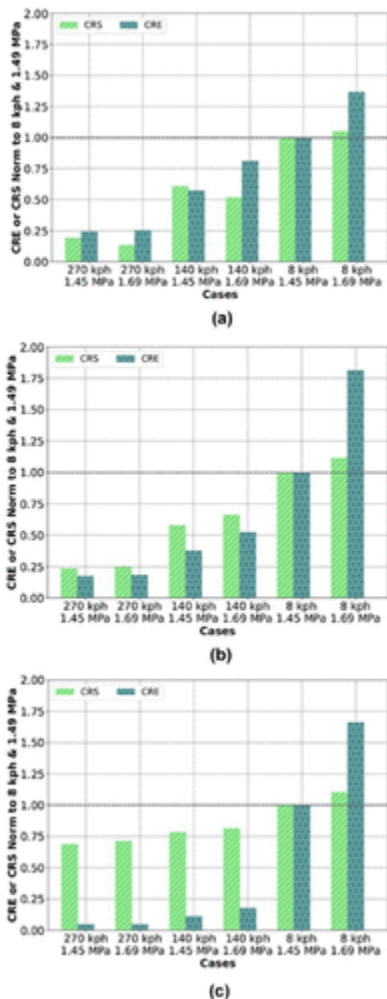


Figure 6. Weighted average of *CRS* and *CRE* for an airfield pavement loaded with A-380 tire considering AC surface temperatures of: (a) -12°C ; (b) 21°C and; (c) 45°C .

Domain Analysis of F-16 Tire Load Cases

The same analysis scheme was implemented for F-16 tire loading cases (Figure 7). As expected, the ratios increased with the decrease in speed and increase in tire-inflation pressure. In contrast to the A-380 cases, reducing the tire load to 72 kN for the F-16 cases led to minimal differences in the ratios when the tire-inflation pressure changed by 12.6%. This elucidates that the considered airfield pavement structure becomes less sensitive to the applied tire–pavement contact stress distribution under low load (given the assumptions described earlier).

However, as nonlinearity begins to govern with increasing temperature, a slight increase in the ratios was observed as the tire-inflation pressures changed. At low speed of 8 kph and AC surface temperature of 45°C, a *CRS* increment of 5.82% resulted within the near-surface region of the AC layer. Corresponding to the same loading case, the *CRE* within the crushed stone base increased by 6.08% as the tire-inflation pressure was altered from 2.14 to 2.41 MPa. Furthermore, the max increase in the weighted average *CRS* and *CRE* values were 4.56% and 2.20%, respectively, for the worst loading scenario.

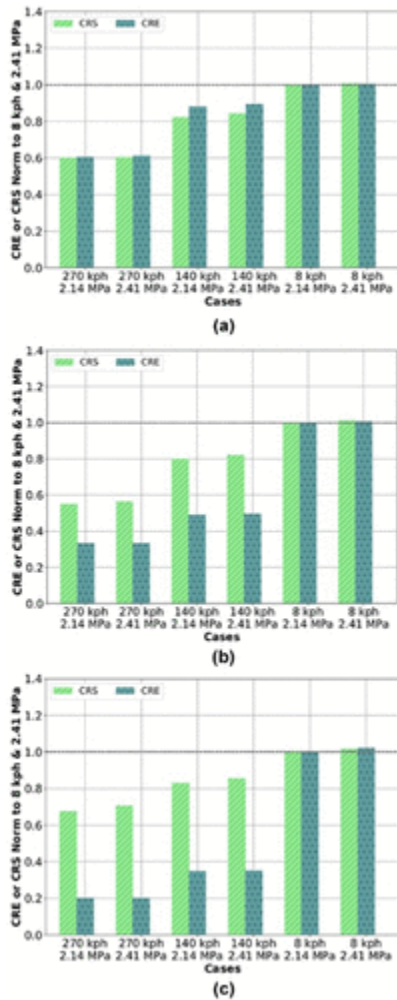


Figure 7. Weighted average of CRS and CRE for an airfield pavement loaded with F-16 tire considering AC surface temperatures of: (a) -12°C ; (b) 21°C and; (c) 45°C .

Summary and Conclusions

Initially applied on highway pavements, the domain analysis aims to capture the direct influence of 3-D and nonuniform tire–pavement contact stresses on pavement responses. As damage initiation may not always be trivial to locate, the proposed method allows the localized region (high stress or strain levels) to be highlighted and inherently penalized via the use of weights, which are defined by the selected failure criteria. Moreover, the combined influence of compression/tension and shear are accounted for in this weighting scheme.

Even though this method has been applied on low-volume and interstate highway flexible pavements considering truck tire loading, the presented study is an initial breakthrough in implementing the proposed analysis on airfield flexible pavements loaded with A-380 and F-16 landing gear. As anticipated, speed and temperature had significant influence on *CRS* and *CRE* ratios for both A-380 and F-16 tire loading cases. Not only did the decrease in speed and increase in temperature increase the cumulative ratios, but the nonlinearity of the problem also became more prevalent at the worst conditions (8 kph and 45°C). The minimal difference in ratios for the F-16 loading cases suggests that the selected airfield pavement structure becomes less sensitive to conditions under low loads.

In contrast to point responses, the critical tensile strain at the bottom of the AC under the slowest speed was minimally influenced by the increase in tire-inflation pressure, wherein the strain increments were 13.6% and 3.1% for A-380 and F-16 cases, respectively. The cumulative ratios, on the other hand, increased up to 81% considering the same loading cases. This is a clear example of the limited capability of point responses to illustrate the influence of tire-inflation pressures, while the domain analysis determined the increase in 3-D stress or strain states via a single scalar. Furthermore, minimal differences in point strains directly influence pavement damage prediction, provided that transfer functions use critical strains as inputs.

Potential adaptation of the presented concepts into flexible airfield pavement design procedures will lead to better representation of actual pavement responses and evolution of pavement damage. Moreover, domain analysis could be easily applied to other scenarios considering varying pavement structures, tire types and configurations, environmental conditions, and tire rolling conditions. Another future parameter to consider is wander, wherein additional FE runs may not be required. Instead, the same output database could be utilized, and wander could be taken into account by shifting the subdomain. Different failure criteria could also be integrated into the domain analysis engine. Lastly, the next step forward is to relate domain analysis results to field measurements with the goal of improving the link between mechanistic responses and damage prediction.

Acknowledgements

This project was conducted in cooperation with the Illinois Center for Transportation. The authors are indebted to Navneet Garg and David Brill for providing the pavement material properties required for the numerical simulations. This study used the Extreme Science and Engineering Discovery Environment (XSEDE), which is supported by National Science Foundation grant number ACI-1548562. We also would like to thank Mahidhar Tatineni for his unyielding assistance in using XSEDE resources.

The Standing Committee on Pavement Structural Modeling and Evaluation peer-reviewed this paper (18-01291).

The contents of this report reflect the view of the authors, who are responsible for the facts and the accuracy of the data presented herein. The contents do not necessarily reflect the official views or policies of the Illinois Center for Transportation. This paper does not constitute a standard, specification, or regulation.

References

1. Advisory Circular 150/5320-6F . Airport Pavement Design and Evaluation. US Department of Transportation, Federal Aviation Administration, 2016.
2. Yoo, P., Al-Qadi, I. L., Elseifi, M., Janajreh, I. Flexible Pavement Responses to Different Loading Amplitudes Considering Layer Interface Condition and Lateral Shear Forces. *International Journal of Pavement Engineering*, Vol. 7, No. 1, 2006, pp. 73–86.
3. Al-Qadi, I. L., Wang, H., Yoo, P. J., Dessouky, S. Dynamic Analysis and In Situ Validation of Perpetual Pavement Response to Vehicular Loading. *Transportation Research Record: Journal of the Transportation Research Board*, 2008. 2087: 29–39.
4. Wang, H., Al-Qadi, I. L., Portas, S., Coni, M. Three-Dimensional Finite Element Modeling of Instrumented Airport Runway Pavement Responses. *Transportation Research Record: Journal of the Transportation Research Board*, 2013. 2367: 76–83.
5. Hernandez, J. A., Gamez, A., Al-Qadi, I. L. Effect of Wide-Base Tires on Nationwide Flexible Pavement Systems: Numerical Modeling. *Transportation Research Record: Journal of the Transportation Research Board*, 2016. 2590: 104–112.
6. Garg, N., Hayhoe, G. F. Asphalt Concrete Strain Responses at High Loads and Low Speeds at the National Airport Pavement Test Facility (NAPTF). In *Advancing Airfield Pavements* (Buttlar, W. G., Naughton, J. E. ed.), American Society of Civil Engineers, Reston, V.A., 2001, pp. 1–14.
7. Al_Qadi, I. L., Portas, S., Coni, M., Lahouar, S. Runway Instrumentation and Response Measurements. *Transportation Research Record: Journal of the Transportation Research Board*, 2012. 2153: 162-169.
8. Roginski, M. J. Effects of Aircraft Tire Pressures on Flexible Pavements. In *Proc., International Conference on Advanced Characterization of Pavement and Soil Engineering*, Athens, Greece, 2007, pp. 1473–1481.
9. Wang, H., Li, M., Garg, N. Simulation of NAPFT High Tire Pressure Tests with Advanced Finite Element Modeling. In *Proc., 2014 FAA Worldwide Airport Technology Transfer Conference*, Galloway, New Jersey, 2014, pp. 1–13.
10. Gamez, A., Hernandez, J. A., Ozer, H., Al-Qadi, I. L. Development of Domain Analysis for Determining Potential Pavement Damage. *ASCE Journal of Transportation Engineering, Part B: Pavements*, 2017, accepted for publication.
11. Yoo, P. J., Al-Qadi, I. L. Effect of Transient Dynamic Loading on Flexible Pavements. *Transportation Research Record: Journal of the Transportation Research Board*, 2007. 1990: 129–140.

12. Al-Qadi, I. L., Yoo, P. J. Effect of Surface Tangential Contact Stresses on Flexible Pavement Response (With Discussion). *Journal of the Association of Asphalt Paving Technologists*, Vol. 76, 2007, pp. 663–695.
13. Yoo, P. J., Al-Qadi, I. L. The Truth and Myth of Fatigue Cracking Potential in Hot-Mix Asphalt: Numerical Analysis and Validation. *Journal of Association of Asphalt Paving Technologists*, Vol. 77, 2008, pp. 549–590.
14. Wang, H., Al-Qadi, I. L. Combined Effect of Moving Wheel Loading and Three- Dimensional Contact Stresses on Perpetual Pavement Responses. *Transportation Research Record: Journal of the Transportation Research Board*, 2009. 2095: 53–61.
15. Xue, W., Weaver, E. Influence of Tyre Configuration on Pavement Response and Predicted Distress. *International Journal of Pavement Engineering*, Vol. 16, No. 6, 2015, pp. 538–548.
16. Gungor, O. E., Hernandez, J. A., Gamez, A., Al-Qadi, I. L., Quantitative Assessment of the Effect of Wide-Base Tires on Pavement Response by Finite Element Analysis. *Transportation Research Record: Journal of the Transportation Research Board*, 2016. 2590: 37–43.
17. Gungor, O. E., Al-Qadi, I. L., Gamez, A., Hernandez, J. A. In-Situ Validation of Three- Dimensional Pavement Finite Element Models. In *The Roles of Accelerated Pavement Testing in Pavement Sustainability* (Aguiar-Moya, J. P., Vargas-Nordbeck, A., Leiva-Villacorta, F., Loria-Salazar, L. G., ed.), Springer, New York, 2016, pp. 145–159.
18. Song, I., Garg, N. High Tire Pressure and Temperature Effects on Hot Mix Asphalt Concrete Permanent Deformation Using Customized Asphalt Pavement Analyzer. In *Proc., 2010 FAA Worldwide Technology Transfer Conference*, Atlantic City, New Jersey, 2010, pp. 1–14.
19. Advisory Circular 150/5370-10G . Standards for Specifying Construction of Airports. US Department of Transportation, Federal Aviation Administration, 2014.
20. Hjelmstad, K. D., Qiu, Z., Kim, J. Elastic Pavement Analysis Using Infinite Elements. *Transportation Research Record: Journal of the Transportation Research Board*, 1997. 1568: 72–76.
21. Hernandez, J. A., Gamez, A., Al-Qadi, I. L., Domain Analysis for Airfield Pavement: Moving Forward from Point Responses. In *Tenth International Conference on the Bearing Capacity of Roads, Railways and Airfields*, Athens, Greece, 2017, pp. 1693-1700
22. Towns, J., Cockerill, T., Dahan, M., Foster, I., Gaither, K., Grimshaw, A., Hazlewood, V., Lathrop, S., Lifka, D., Peterson, G. D.. XSEDE: Accelerating Scientific Discovery. *Computing in Science & Engineering*, Vol. 16, No. 5, 2014, pp. 62–74.
23. Hernandez, J. A., Al-Qadi, I. L., Airfield Pavement Response Caused by Heavy Aircraft Takeoff: Advanced Modeling for Consideration of Wheel Interaction. *Transportation Research Record: Journal of the Transportation Research Board*, 2015. 2471: 40–47.
24. Hernandez, J., Gamez, A., Al-Qadi, I. L., De Beer, M. Analytical Approach for Predicting Three-Dimensional Tire-Pavement Contact Load. *Transportation Research Record: Journal of the Transportation Research Board*, 2014. 2456: 75-84.
25. Guo, K., Lu, D. UniTire: Unified Tire Model for Vehicle Dynamic Simulation. *Vehicle System Dynamics*, Vol. 45, No. S1, 2007, pp. 79–99.
26. Wang, H., Al-Qadi, I. L. Impact of Non-Uniform Aircraft Tire Pressure on Airfield Pavement Responses. In *Transportation and Development Institute Congress 2011: Integrated Transportation and Development for a Better Tomorrow*, Chicago, Illinois, 2011, pp. 844–853.

27. Lindsley, N. H., Medzorian, J. P., Lay, M. K., Marcy, W. W. Effects of Flywheel Curvature on Aircraft Tire Footprint Behavior. Technical Paper 952020. SAE, Warrendale, Pennsylvania, 1995.
28. Hernandez, J. A., Al-Qadi, I. L., De Beer, M. Impact of Tire Loading and Tire Pressure on Measured 3D Contact Stresses. In *Airfield and Highway Pavement 2013: Sustainable and Efficient Pavements* (Al-Qadi, I. L., Murrell, S. ed.), American Society of Civil Engineers, Reston, V.A., 2013, pp. 551–560.
29. Hernandez, J. A., Al-Qadi, I. L. Hyperelastic Modeling of Wide-Base Tire and Prediction of Its Contact Stresses. *Journal of Engineering Mechanics*, Vol. 142, No. 2, 2015, p. 04015084.
30. Hernandez, J. A., Gamez, A., Al-Qadi, I. L., Effect of Wide-Base Tires on Nationwide Flexible Pavement Systems: Numerical Modeling. *Transportation Research Record: Journal of the Transportation Research Board*, 2016. 2590: 104–112.
31. Wang, H., Al-Qadi, I. Near-Surface Pavement Failure under Multiaxial Stress State in Thick Asphalt Pavement. *Transportation Research Record: Journal of the Transportation Research Board*, 2010. 2154: 91–99.